SUPPLEMENTARY MATERIAL

Personalized Connectome Mapping to Guide Targeted Therapy and Promote Recovery of Consciousness in the Intensive Care Unit

Brian L. Edlow[1,2], Megan E. Barra[1,3], David W. Zhou[1,4], Samuel B. Snider[1], Zachary D. Threlkeld[1,5], John E. Kirsch[2], Suk-tak Chan[2], Steven L. Meisler[1], Thomas P. Bleck[6], Joseph J. Fins[7,8,9], Joseph T. Giacino[10], Leigh R. Hochberg[1,11,12], Ken Solt[13], Emery N. Brown[4,13], and Yelena G. Bodien[1,10]

Author Affiliations:
[1] Center for Neurotechnology and Neurorecovery, Department of Neurology, Massachusetts General Hospital, Boston, MA
[2]Athinoula A. Martinos Center for Biomedical Imaging, Massachusetts General Hospital, Charlestown, MA
[3] Department of Pharmacy, Massachusetts General Hospital, Boston, MA
[4] Department of Brain and Cognitive Sciences, Massachusetts Institute of Technology, Cambridge, MA
[5] Department of Neurology and Neurological Sciences, Stanford School of Medicine, Stanford, CA
[6] Department of Neurology, Northwestern University Feinberg School of Medicine, Chicago, IL
[7] Division of Medical Ethics and Consortium for the Advanced Study of Brain Injury (CASBI), Weill Cornell Medical College, New York, NY
[8] The Rockefeller University
[9] Solomon Center for Health Law and Policy, Yale Law School, New Haven, CT
[10] Department of Physical Medicine and Rehabilitation, Spaulding Rehabilitation Hospital, Boston, MA
[11] School of Engineering and Carney Institute for Brain Science, Brown University, Providence, RI
[12] Veterans Affairs RR&D Center for Neurorestoration and Neurotechnology, VA Medical Center, Providence, RI
[13] Department of Anesthesiology, Massachusetts General Hospital, Boston, MA

Corresponding author:
B.L. Edlow
bedlow@mgh.harvard.edu

Supplementary Methods

Acquisition and Processing of EEG Data

EEG data are acquired in the Massachusetts General Hospital Neurosciences Intensive Care Unit using a 19-electrode clinical XLTEK EEG system (Natus Medical Inc.; Pleasanton, CA) at a 200- or 256-Hz sampling rate. We the process the data using EEGlab [1] and customized MATLAB code. All recordings are filtered (third-order Butterworth, zero-phase shift digital filter, 1-30 Hz) and re-referenced using the Hjorth Laplacian transform to optimize spatial localization and avoid contaminating activity at the reference [2]. We perform artifact rejection with EEGlab using independent component analysis. Following artifact rejection, we estimate the power spectral density of the voltage activity recorded at each electrode. Absolute power estimates are averaged within four frequency bands: delta [1-3 Hz], theta [4-7 Hz], alpha [8-13 Hz], beta [14-30 Hz], allowing calculation of the alpha-delta ratio. Additional details regarding EEG acquisition and processing have been previously described [3].

Acquisition and Processing of High Angular Resolution Diffusion Imaging (HARDI) Data

All HARDI data acquisition and processing methods, as well as the CP calculation, have been previously described by our group [4]. Patients are scanned on a 3 Tesla Skyra MRI scanner (Siemens Medical Solutions) in the Massachusetts General Hospital Neurosciences Intensive Care Unit using a 32-channel head coil. HARDI sequence parameters are 2 mm isotropic voxels, 60 diffusion-encoded volumes (b=2000 s/m^2), 10 “b0” volumes (b=0 s/m^2) and a 220 mm FOV. The scans are acquired using simultaneous

multi-slice (SMS) imaging [5] with TR=6700 ms, TE=100 ms, echo spacing 0.7 ms, and epi factor 110.

We pre-process the HARDI data in FSL (FMRIB, Oxford, UK), which includes brain extraction, eddy current and bulk motion correction. Diffusion parameters are estimated using bedpostx with default parameter settings. Probabilistic tractography is performed using probrackx2 with 5000 samples per voxel, curvature threshold of 80°, max steps 2000, step length 0.5 mm, minimum length 0, no anisotropy constraining, and no distance correction.

To calculate a connectivity probability (CP) between specific seed and target regions of interest (ROI), we use each target ROI as a waypoint and termination mask in probtrackx2. We then repeat the analysis swapping seed and target. The CP is then calculated as a weighted average of the relative number of tracts reaching target from seed and relative number of tracts reaching seed from target:

$$CP = \frac{k1 + k2}{n1 + n2}$$

where

$k1 = tracts\ from\ seed\ reaching\ target$

$k2 = tracts\ from\ target\ reaching\ seed$

$n1 = 5000 \times seed\ voxels$

$n2 = 5000 \times target\ voxels$

This formula models CP as binomial distribution with each $p_i = k_i/n_i$ derived from k_i tracts reaching the relative target from n_i trials (5000 X seed voxels). With two samples (seed-to-target and target-to-seed), the resulting P (CP) is a weighted average of the two p_i, each weighted by n_i trials.

Calculation of the Predictive Biomarker, S_{VTA}

Once CP values are generated for each seed-target pair (e.g. ventral tegmental area [VTA] and target nodes of the default mode network [DMN]), these CP values are entered into an adjacency matrix for graph theoretical analysis using the Matlab-based Brain Connectivity Toolbox [6]. We use graph theoretic analysis to derive the hub strength, S_{VTA}, of the VTA. This continuous variable represents the sum of the CPs of structural connections between the VTA and other nodes of the ascending arousal network (AAN) and the default arousal network (DMN), as measured by high angular resolution diffusion imaging (HARDI). S_{VTA} is a unitless value [7] calculated as $S_{VTA} = \sum_{j=1}^{N} a_{VTAj} w_{VTAj}$ where nodes are numbered *j* to *N*, a_{VTAj} is the presence (*a*=1) or absence (*a*=0) of a connection, and w_{VTAj} is the *CP* between the VTA and node j [6]. This metric has been used as a measure of a node's "hubness" in previous brain network studies [8-11]. S_{VTA} calculation will be performed using the Brain Connectivity Toolbox in MATLAB (Natick, MA) [6].

Acquisition and Processing of Resting-state Functional MRI (rs-fMRI) Data

All rs-fMRI acquisition and processing procedures have been previously described by our group [12, 13], with the exception of the new SMS rs-fMRI sequence described here.

Patients undergo rs-fMRI on the same 3 Tesla Skyra MRI scanner and with the same 32-channel head coil used for HARDI data acquisition. For registration, we acquire T_1-weighted multi-echo magnetization prepared gradient echo (MEMPRAGE) images in the sagittal plane: 176 slices, echo time=1.69, 3.55, 5.41, 7.27 ms, repetition time=2530 ms, 1.0 mm^3 isotropic resolution, matrix size=256x256, flip angle=7°, inversion time=1200-1300 ms [14]. We perform rs-fMRI using an SMS blood-oxygen-level-dependent (BOLD) sequence with 622 seconds of data acquisition, 72 axial slices, echo time=30 ms, repetition time=1250 ms, voxel size=2.0x2.0x2.0 mm, and matrix size=106x106. Prior to rs-fMRI, we instruct each subject to "keep your eyes open and relax."

We process the BOLD rs-fMRI data using the CONN functional connectivity toolbox (www.nitrc.org/projects/conn) [15] for slice-timing correction, realignment, structural segmentation, normalization into Montreal Neurological Institute (MNI-152) space, and smoothing with a 6 mm full-width at half-maximum Gaussian kernel. We use the artifact rejection tool (ART) to reject outlier volumes satisfying at least one of the following thresholds: normalized global BOLD signal $Z \geq 3.0$, absolute subject motion $\geq$ 0.5 mm, absolute subject rotation $\geq$ 0.05 radians, scan-to-scan motion $\geq$ 1.0 mm, and scan-to-scan rotation $\geq$ 0.02 radians. For denoising, we use CSF and white matter principal components as nuisance covariates in accordance with the anatomical component-based noise correction method (aCompCor) [16, 17]. After denoising, we isolate low-frequency fluctuations with a low-pass temporal filter (0.008 to 0.09Hz).

We investigate functional connectivity using a seed-based approach, in which the mean time series in a seed region is compared with the time series of all other voxels in the brain. For the VTA seed, we use the Harvard Ascending Arousal Network atlas. For

the DMN, we use four 10-mm diameter spherical seeds: one in the medial prefrontal cortex (MPFC), one in the posterior cingulate cortex (PCC), and one in each of the left and right lateral parietal cortices (LP), as described by Raichle [18]. We generate a mean DMN time series by averaging the time series among the four DMN seeds [19]. To generate $Z_{VTA\text{-}DMN}$, we calculate the Pearson's correlation coefficient between the time series of the VTA seed and the mean time series of the DMN seeds, followed by Fisher *Z*-transformation for inter-subject comparison. Additional details regarding rs-fMRI data acquisition and processing can be found in Threlkeld et al. [12].

Development of a Normative Connectome Dataset

To establish the normative dataset of S_{VTA}, $Z_{VTA\text{-}DMN}$, and *alpha-delta* values, we will enroll 50 healthy adult volunteers aged ≥ 18 years old.

Data Analysis:

On Day 0, S_{VTA}, *alpha-delta ratio*, and $Z_{VTA\text{-}DMN}$ will be measured for each patient. We will define a threshold for "preserved S_{VTA}" – the lower bound of the 95% confidence interval from the 50-subject healthy control normative dataset – above which patients will be phenotyped as likely responders to IV MPH in STIMPACT Phase 2a. Because the STIMPACT Phase 1 trial is focused on safety and dose-finding, all patients will receive IV MPH, regardless of their S_{VTA} measures. Rs-fMRI data will be analyzed to calculate $Z_{VTA\text{-}DMN}$ using our published methods [12].

Power Calculation for STIMPACT Phase 1

We aim to detect, with high probability, a drug-related serious adverse event (SAE) that would prevent us from moving to Phase 2a. Specifically, we designed the trial to have an 90% chance of detecting any drug-related SAE that occurs with a frequency of ≥ 10%. Based on these criteria, we used the binomial equation to calculate our sample size: $1-(1-p)^n=y$, where p=drug-related SAE rate, n=number of subjects, and y=chance of detecting the SAE. Using a drug-related SAE rate of 10% (p=0.10) and requiring a 90% probability of detecting the SAE at least once (y=0.90), we calculate that a 22-subject cohort will be necessary to enroll in Phase 1. We will determine the frequency of drug-related SAEs at each dose, and if two drug-related SAEs occur at a dose (frequency~10%), that dose and all higher doses will be removed from the trial. If two drug-related SAEs occur at the lowest dose, the trial will be stopped and Phase 1 will be repeated at a lower dose range.

Physiological Monitoring and Analysis

We acquire cardiac and respiratory waveforms through a pulse-oximeter and respiratory bellow (Physiological Monitoring Unit, Siemens Medical, Erlangen, Germany), respectively, when patients are at rest during the rs-fMRI scanning. It is believed that the pulsatile nature of blood flow in the brain, as well as motion and magnetic field variations due to respiration, can cause artifacts in BOLD signal [20, 21]. Fluctuations relating to respiratory variation [22] and heart rate [23] have been proposed as 'physiological noise' to be removed from BOLD signals in healthy subjects. However, the contribution of these fluctuations to BOLD signals in patients with acute brain injuries is not completely understood. Therefore, before respiratory variation and heart rate related

fluctuations are removed, we examine the dynamic coupling between rs-fMRI signal changes and these fluctuations.

We use wavelet transform coherence to examine the dynamic interaction between BOLD signal changes and respiratory variation/heart rate in the time-frequency domain. Wavelet transform coherence is a method for analyzing the coherence and phase lag between two time courses as a function of both time and frequency [24, 25]. The Matlab wavelet cross-spectrum toolbox developed by Grinsted et al. [25] is used. An example of squared wavelet coherence between BOLD signal changes and respiratory variation in the left ventral diencephalon from a representative healthy subject and a representative patient with acute severe TBI is shown in Figure 5. An example of squared wavelet coherence between BOLD signal changes and heart rate in the left ventral diencephalon from the same subjects is shown in Supplementary Figure 2.

In Figure 5, the time series of respiratory variation and ΔBOLD in left ventral diencephalon are shown in the left column. By visual inspection, there are fast and slow components of the fluctuations in the time series which are contributed by different underlying physiological processes. Squared wavelet coherence is plotted with x-axis as time (i.e. the time from the onset of resting-state run) and y-axis as scale which has been converted to its equivalent Fourier period to show the distribution of the fast and slow components of fluctuations (in the unit of seconds) in the time series (Figure 5, middle column). Fourier period of 4 seconds indicates fast component of fluctuations and that of 128 seconds (or ~2 minutes) indicates slow component of fluctuations. The strength of interaction between respiratory variation and ΔBOLD is demonstrated by the magnitude of coherence in the range from 0 to 1, where warmer color represents stronger coherence

(close to 1) and cooler color represents weaker coherence (close to 0). The magnitude of coherence can be conceptualized as a localized correlation coefficient between respiratory variation and ΔBOLD, where the x-coordinate in the coherence map provides the information on how fast the rate of fluctuations when respiratory variation interacts with ΔBOLD, and y-coordinate provides the time when this interaction occurs over the resting-state scan. The direction of the arrows in the coherence map provides the polarity of correlation. A positive correlation is represented by the arrow pointing between 12 o'clock and 6 o'clock positions on the right half of the clock (i.e. phase lag of $0\pm\pi/2$ between the two time series), while the arrow pointing to the left half of the clock represents a negative correlation (i.e. phase lag of $0\pm\pi/2$ between the two time series). Significant interaction between respiratory variation and ΔBOLD is only considered when the magnitude of coherence exceeds 95% significance level (i.e. the area within thick contour of the unfaded region). Therefore, a significantly strong positive interaction between respiratory variation and ΔBOLD occurs at the locations where small areas in dark red color within thick contour and a rightward pointing arrow are found.

In the representative healthy subject, the components of fluctuations from respiratory variation and ΔBOLD that oscillate at the rates of 16-32 seconds (~0.03 to 0.063 Hz) and 64 seconds (~0.016 Hz) have significantly strong interaction at 200-400 seconds from the onset of the resting-state scan, suggesting that this part of the respiratory variation signals may have influence on the ΔBOLD signals. To simplify the coherence results from two dimensions in squared wavelet coherence to one dimension, we average and normalize the significant coherence between the two time series over the time on x-axis (Figure 5, right column). Although we lose information about when the

interaction occurs, the features of oscillations in terms of frequency for the interaction between respiratory variation and ΔBOLD are retained. While increased coherence is found between respiratory variation and ΔBOLD at the frequency range of 0.008 to 0.063 Hz in the healthy subject, the coherence between respiratory variation and ΔBOLD in the same frequency range is diminished in the acute severe TBI subject.

To remove the physiological noise contributed by the respiratory and cardiac activities, we use the RETROICOR algorithm [26] through the Physiological Noise Modeling (PNM) module in the FMRIB Software Library (FSL) [27, 28]. The time series of cardiac and respiratory waveforms are collected and aligned with the MRI volumes using trigger signals from the scanner. Peaks and troughs of the cardiac and respiratory cycles on the physiological time series are determined using a custom Matlab function (Matlab R2014a, Mathworks, Inc., Natick, MA, USA) and corrected on the graphical user interface incorporated in the function. For the cardiac time series, the peaks and troughs indicating the systolic and end-diastolic phases of the cardiac cycles, respectively, are determined. For the respiratory time series, the peaks and troughs indicating end-inspiration and end-expiration, respectively, are determined. This step makes enables the FSL software to calculate the cardiac phases and respiratory phases on the physiological time series with pre-determined peaks and troughs. While the cardiac phase advances linearly from 0 to 2π during the time interval between two consecutive cardiac peaks and is reset to zero for the next cycle, the inspiratory phase spans 0 to π and the expiratory phase spans 0 to -π for each respiratory cycle (Supplementary Figure 1). Both the time series of cardiac phases and respiratory phases are used in RETROICOR to remove physiological noise in the rs-fMRI dataset.

STIMPACT Phase 1 Statistical Analysis

We define a pharmacodynamic response for each patient by an MPH-related change in $Z_{VTA\text{-}DMN}$ or *Alpha/delta* relative to the patient's own baseline variance in these biomarkers. To test the effect of IV MPH on $Z_{VTA\text{-}DMN}$, we will measure changes in $Z_{VTA\text{-}DMN}$ at baseline (Day 0) and during treatment (Day 4). On Day 0 and Day 4, $Z_{VTA\text{-}DMN}$ will be compared between two 10-minute rs-fMRI time periods: the first 10 minutes of the scan versus minutes 10-20 of a subsequent 30-minute scan. We select minutes 10-20 because positron emission tomography data indicate that the effects of IV MPH peak in the brain between minutes 10 and 20 [29]. The response criteria will be based on a single-subject comparison of the difference between $\Delta Z_{VTA\text{-}DMN(Day\ 0)}$ and $\Delta Z_{VTA\text{-}DMN\ (Day\ 4)}$ using the following formula: $(\Delta Z_{VTA\text{-}DMN\ (Day\ 4)} - \Delta Z_{VTA\text{-}DMN\ (Day\ 0)}) / \sqrt{n} > 1.96$, where n = the number of measurements (i.e. 4). Thus, if $\Delta Z_{VTA\text{-}DMN\ (Day\ 4)} - \Delta Z_{VTA\text{-}DMN\ (Day\ 0)} > 3.92$ we will conclude that the patient is a responder. This is the criterion for statistical significance at an alpha level of 0.05 if *Z* has a variance of 1. To test the effect of IV MPH on *Alpha/delta*, we will use a similar approach, except that *Alpha/delta* will be derived by averaging across each second of EEG data for each 10-minute period. The response criteria will be based on a single-subject comparison of the difference between $\Delta Alpha/delta_{\ (Day\ 3)}$ and $\Delta Alpha/delta_{\ (Day\ 0)}$ using the following formula: $(\Delta Alpha/delta_{\ (Day\ 3)} - \Delta Alpha/delta_{\ (Day\ 0)}) / \sqrt{n} > 1.96$, where n = the number of measurements (i.e. 4). Therefore, if $\Delta Alpha/delta_{\ (Day\ 3)} - \Delta Alpha/delta_{\ (Day\ 0)} > 3.92$ we will conclude that there is a significant effect of IV MPH on *Alpha/delta* at an alpha level of 0.05.

Predefined Criteria for Progressing to STIMPACT Phase 2A

We will proceed from Phase 1 to Phase 2a if predetermined safety *and* pharmacodynamic biomarker criteria are met. These criteria yield three potential outcomes for STIMPACT Phase 1 (Supplementary Fig. 3): 1) IV MPH is safe and ≥ 10% of the 22 patients show a response in *alpha/delta* or $Z_{VTA\text{-}DMN}$ → we will continue to Phase 2a at the maximum tolerated dose; 2) IV MPH is not safe, even at the lowest dose → we will repeat Phase 1 in 22 new patients at a lower dose range; 3) IV MPH is safe, but ≤ 10% show a response → we will repeat Phase 1 in 22 patients at a higher dose range *and* we will leverage the flexibility of the CCTP by testing additional graph theory measures as pharmacodynamic biomarkers. For example, if *Alpha/delta* does not respond to IV MPH, we will test for changes in hub strength within cortical nodes that correspond to DMN hubs. Similarly, if $Z_{VTA\text{-}DMN}$ does not respond to IV MPH, we will test for a change in Z_{DMN}, which we have shown correlates with level of consciousness in the ICU [12]. Hence, the CCTP provides alternate approaches at each stage of trial design while maintaining the central focus on connectome-based measures of therapeutic responses. The study design for Phase 2A will be finalized upon completion of Phase 1.

Phase 2a Study Design Considerations

Phase 2a will be a single-center, double-blinded, randomized, cross-over design trial. The predictive biomarker (S_{VTA}) and baseline pharmacodynamic biomarker data (*alpha-delta* and $Z_{VTA\text{-}DMN}$) will again be acquired on Day 0. Patients will then be randomized to receive alternating daily doses of IV MPH or placebo on Days 1-2 (i.e. MPH/Placebo or Placebo/MPH). On Days 1-2, *alpha-delta* ratio will be measured before and after IV MPH

and placebo. On Day 3, all patients will receive IV MPH during an rs-fMRI scan for $Z_{VTA\text{-}DMN}$ measurement. The primary endpoint for Phase 2a will be whichever biomarker demonstrates a larger group-level response to IV MPH in Phase 1 (*Alpha/delta* or $Z_{VTA\text{-}DMN}$). The primary hypothesis of STIMPACT Phase 2a is that preserved S_{VTA} predicts a pharmacodynamic biomarker response to IV MPH relative to placebo. Secondary endpoints will be the pharmacodynamic biomarker with the lower group-level effect size in Phase 1, as well as a clinical biomarker, the change in level of consciousness on behavioral assessment with the Coma Recovery Scale-Revised. The predetermined criterion for proceeding from Phase 2a to Phase 2b will be that ≥ 10% of patients show a pharmacodynamic biomarker response to IV MPH. If ≥ 10% of patients are responders *and* preserved S_{VTA} predicts a response, then only patients with preserved S_{VTA} will be enrolled in Phase 2b. We will have thus demonstrated the CCTP's utility by creating an efficiently designed late-phase clinical trial. If ≥ 10% of patients respond to IV MPH but S_{VTA} does *not* predict a response, we will still proceed to Phase 2b because of the potential benefit of IV MPH to patients. However, leveraging the flexibility of the CCTP, we will test whether other graph theory properties, alone or in combination, predict MPH responses.

Phase 2a Statistical Considerations

We will test the hypothesis that preserved S_{VTA} independently predicts an MPH response using logistic regression and correcting for the following covariates: 1) level of consciousness at enrollment; 2) days post-injury at enrollment; 3) age; 4) sex; and 5) level of sedation. The sample size for Phase 2a will be based upon whichever

pharmacodynamic marker – *alpha-delta* or $Z_{VTA\text{-}DMN}$ – yields the larger effect size in Phase 1. Given our preliminary data, and assuming an MPH response rate of 10%, we will need to enroll 40 patients to test a logistic model with "IV MPH response" as the dependent binary variable. This model will provide 80% power to detect the contribution of S_{VTA} to an IV MPH response, with an alpha level of 0.05 and an odds ratio of at least 4, which is the standard clinically meaningful cut-off.

If the logistic regression yields an S_{VTA} coefficient that is statistically significant, we will conclude that S_{VTA} predicts an MPH response. We acknowledge that carry-over effects (i.e. MPH effects persisting until placebo administration) are a concern in cross-over studies. However, carry-over effects are unlikely because there will be 24 hours between drug and placebo, which is more than 16 half-lives of IV MPH [29]. Furthermore, if a patient recovers consciousness after IV MPH, that patient will not receive placebo the next day, eliminating carry-over effects for these responders.

Supplementary References

1. Delorme A and Makeig S, EEGLAB: an open source toolbox for analysis of single-trial EEG dynamics including independent component analysis. J Neurosci Methods, 2004; 134: 9-21.
2. Lepage KQ, Kramer MA, and Chu CJ, A statistically robust EEG re-referencing procedure to mitigate reference effect. J Neurosci Methods, 2014; 235: 101-16.
3. Edlow BL, Chatelle C, Spencer CA, et al., Early detection of consciousness in patients with acute severe traumatic brain injury. Brain, 2017; 140: 2399-2414.
4. Snider SB, Bodien YG, Bianciardi M, et al., Disruption of the ascending arousal network in acute traumatic disorders of consciousness. Neurology, 2019; 93: e1281-e1287.
5. Setsompop K, Gagoski BA, Polimeni JR, et al., Blipped-controlled aliasing in parallel imaging for simultaneous multislice echo planar imaging with reduced g-factor penalty. Magn Reson Med, 2012; 67: 1210-24.
6. Rubinov M and Sporns O, Complex network measures of brain connectivity: uses and interpretations. Neuroimage, 2010; 52: 1059-69.
7. Barrat A, Barthelemy M, Pastor-Satorras R, et al., The architecture of complex weighted networks. Proc Natl Acad Sci U S A, 2004; 101: 3747-52.
8. Achard S, Delon-Martin C, Vertes PE, et al., Hubs of brain functional networks are radically reorganized in comatose patients. Proc Natl Acad Sci U S A, 2012; 109: 20608-13.
9. Aerts H, Fias W, Caeyenberghs K, et al., Brain networks under attack: robustness properties and the impact of lesions. Brain, 2016; 139: 3063-3083.

10. Caeyenberghs K, Leemans A, Leunissen I, et al., Topological correlations of structural and functional networks in patients with traumatic brain injury. Front Hum Neurosci, 2013; 7: 726.
11. Castellanos NP, Leyva I, Buldu JM, et al., Principles of recovery from traumatic brain injury: reorganization of functional networks. Neuroimage, 2011; 55: 1189-99.
12. Threlkeld ZD, Bodien YG, Rosenthal ES, et al., Functional networks reemerge during recovery of consciousness after acute severe traumatic brain injury. Cortex, 2018; 106: 299-308.
13. Bodien YG, Threlkeld ZD, and Edlow BL, Default mode network dynamics in covert consciousness. Cortex, 2019.
14. van der Kouwe AJW, Benner T, Salat DH, et al., Brain morphometry with multiecho MPRAGE. Neuroimage, 2008; 40: 559-569.
15. Whitfield-Gabrieli S and Nieto-Castanon A, Conn: a functional connectivity toolbox for correlated and anticorrelated brain networks. Brain Connect, 2012; 2: 125-41.
16. Behzadi Y, Restom K, Liau J, et al., A component based noise correction method (CompCor) for BOLD and perfusion based fMRI. Neuroimage, 2007; 37: 90-101.
17. Muschelli J, Nebel MB, Caffo BS, et al., Reduction of motion-related artifacts in resting state fMRI using aCompCor. Neuroimage, 2014; 96: 22-35.
18. Raichle ME, The restless brain. Brain Connect, 2011; 1: 3-12.

19. Demertzi A, Antonopoulos G, Heine L, et al., Intrinsic functional connectivity differentiates minimally conscious from unresponsive patients. Brain, 2015; 138: 2619-31.

20. Glover GH and Lee AT, Motion artifacts in fMRI: comparison of 2DFT with PR and spiral scan methods. Magn Reson Med, 1995; 33: 624-35.

21. Noll DC and Schneider W, Theory, simulation, and compensation of physiological motion artifacts in functional MRI. IEEE Proceedings of 1st International Conference on Image Processing, 1994.

22. Birn RM, Diamond JB, Smith MA, et al., Separating respiratory-variation-related fluctuations from neuronal-activity-related fluctuations in fMRI. Neuroimage, 2006; 31: 1536-48.

23. Shmueli K, van Gelderen P, de Zwart JA, et al., Low-frequency fluctuations in the cardiac rate as a source of variance in the resting-state fMRI BOLD signal. Neuroimage, 2007; 38: 306-20.

24. Torrence C and Compo GP, A Practical Guide to Wavelet Analysis. Bulletin of the American Meteorological Society, 1998; 79: 61-78.

25. Grinsted A, Moore JC, and Jevrejeva S, Application of the cross wavelet transform and wavelet coherence to geophysical time series. Nonlinear Processes in Geophysics, 2004; 11.

26. Glover GH, Li TQ, and Ress D, Image-based method for retrospective correction of physiological motion effects in fMRI: RETROICOR. Magn Reson Med, 2000; 44: 162-7.

27. Smith SM, Jenkinson M, Woolrich MW, et al., Advances in functional and structural MR image analysis and implementation as FSL. Neuroimage, 2004; 23 Suppl 1: S208-19.

28. Brooks JC, Beckmann CF, Miller KL, et al., Physiological noise modelling for spinal functional magnetic resonance imaging studies. Neuroimage, 2008; 39: 680-92.

29. Swanson JM and Volkow ND, Serum and brain concentrations of methylphenidate: implications for use and abuse. Neurosci Biobehav Rev, 2003; 27: 615-21.

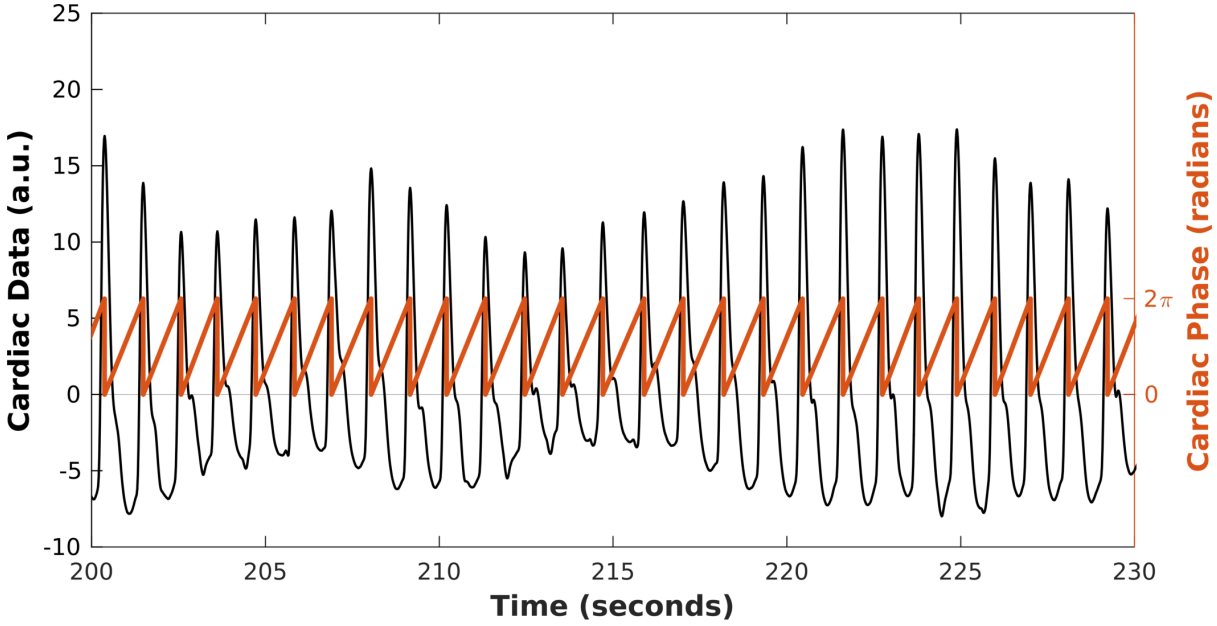

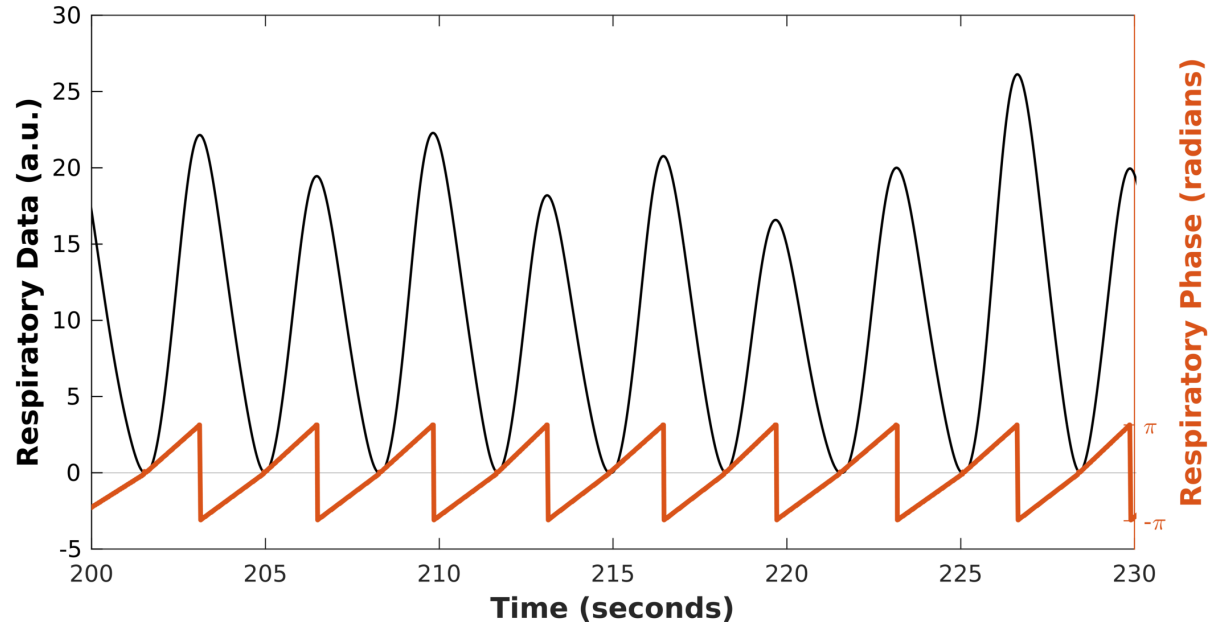

Supplementary Figure 1. Time series of cardiac (upper panel) and respiratory data (lower panel) acquired simultaneously with the acquisition of resting state BOLD data. The peaks in cardiac time series serve as surrogate of R peaks in ECG, while the peaks in respiratory time series indicate peak inspiration and the troughs represent end expiration. The cardiac phase used in RETROICOR advances linearly from 0 to 2π during each R-R interval and is reset to 0 for the next cycle. The inspiratory phase spans 0 to π and the expiratory phase spans 0 to $-\pi$.

Time Series of Heart Rate and ΔBOLD in Left Ventral Diencephalon

Coherence between Heart Rate and ΔBOLD

Time-averaged Coherence at Different Phase Lags

Healthy Subject

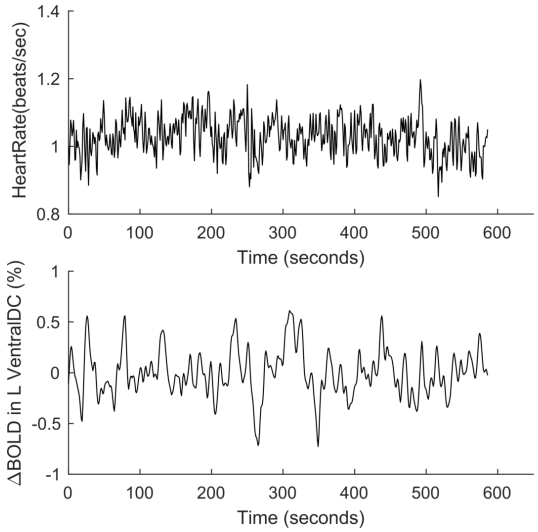

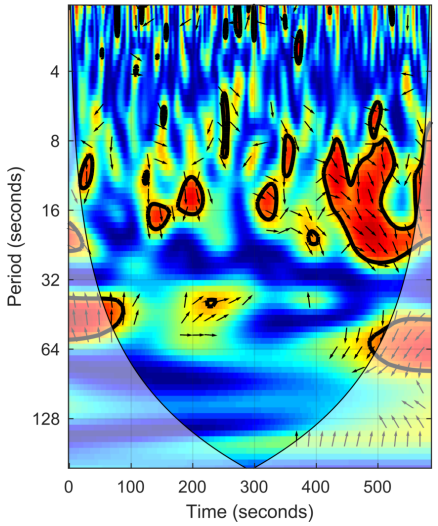

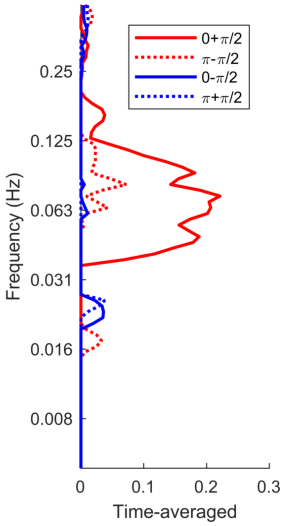

Acute Severe TBI

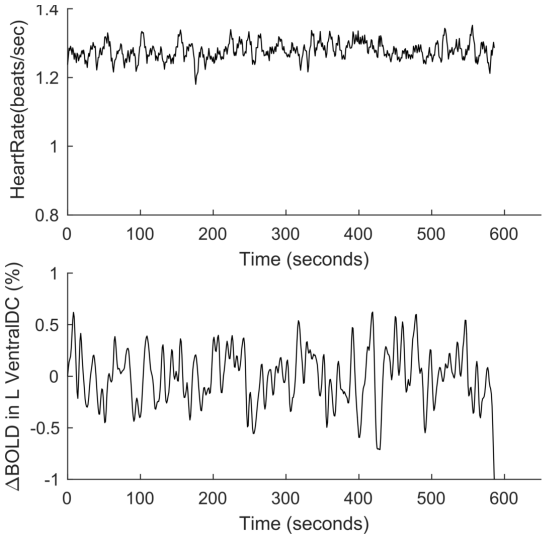

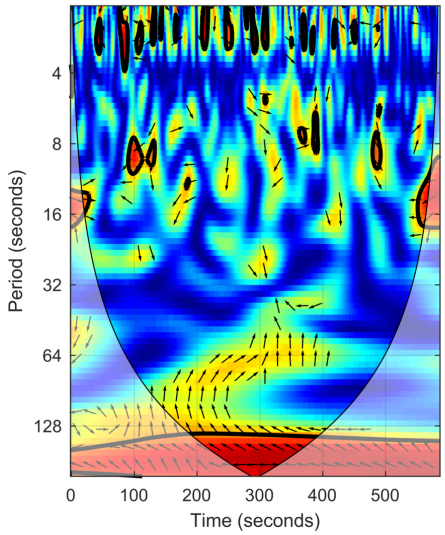

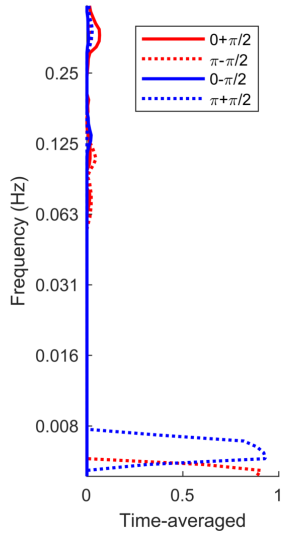

Supplementary Figure 2. Coherence between heart rate and BOLD signal changes in a representative control subject (upper panel) and a representative patient (lower panel). Time series of heart rate and ΔBOLD in the left ventral diencephalon are shown in the left column. The dynamic interaction between heart rate and ΔBOLD is demonstrated by the squared wavelet coherence between the time series of heart rate and ΔBOLD, as shown in the middle column. The magnitude of coherence ranges between 0 and 1, where a warmer color represents stronger coherence and cooler color represents weaker coherence. Significant coherence between heart rate and ΔBOLD occurs in the area defined by thick contour of the unfaded region. The x-coordinate of the area provides information on the duration of the oscillating cycle when heart rate interacts with ΔBOLD, and the y-coordinate provides the time when this interaction occurs during the resting state fMRI scan. The simplified format of coherence between heart rate and ΔBOLD is shown in the right column, with the features of oscillations shown in terms of frequency only. While increased coherence is found between heart rate and ΔBOLD at the frequency range of 0.031-0.125Hz in the healthy subject, the coherence between heart rate and ΔBOLD in the same frequency range is diminished in the patient with acute severe TBI. Compared to the healthy subject, the resting state BOLD signal changes have less influence from heart rate in the patient with acute severe TBI.

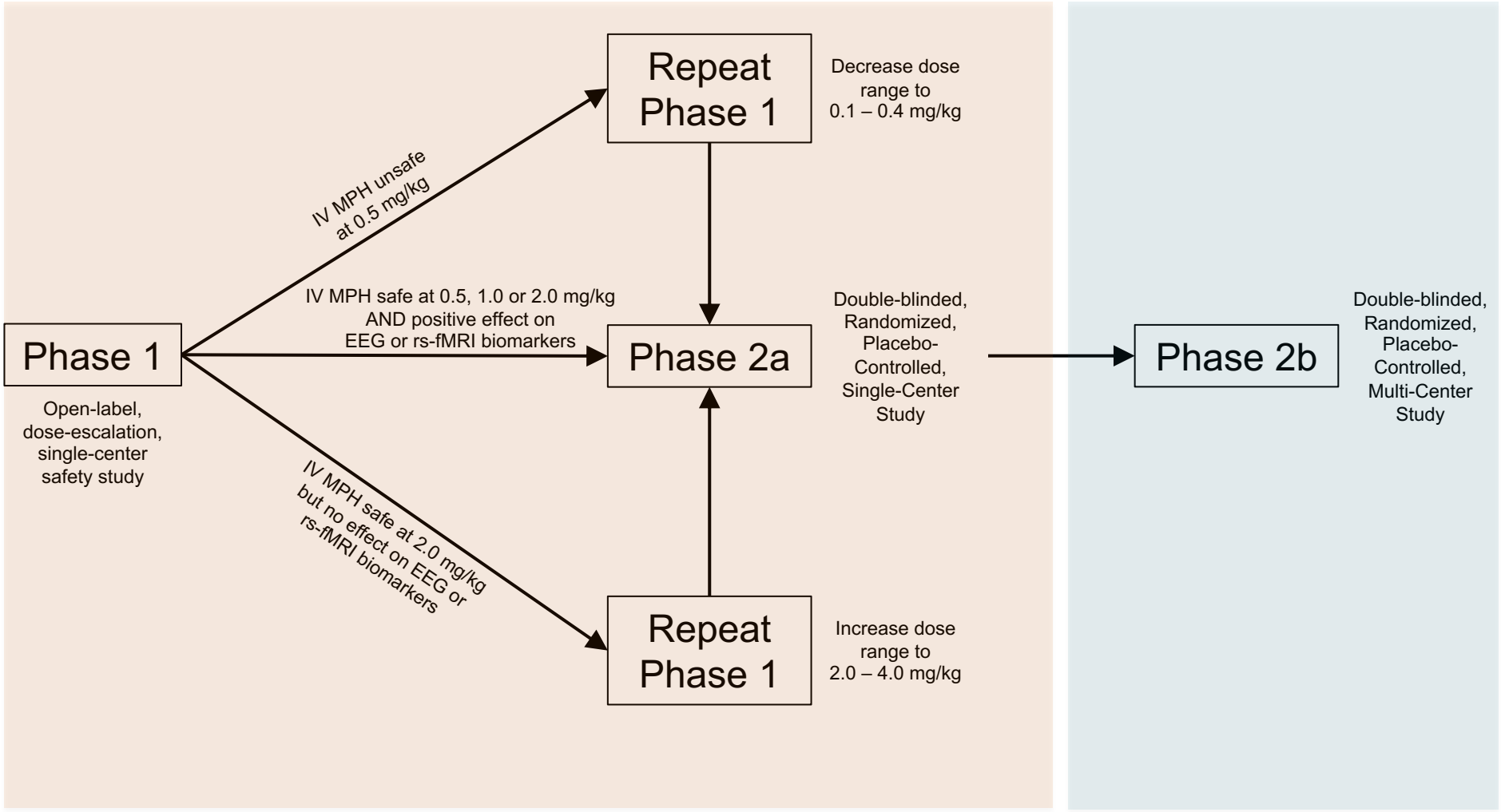

Supplementary Figure 3. Decision tree for Phases 1, 2a, and 2b of the STIMPACT Trial. Abbreviations: EEG = electroencephalography; IV MPH = intravenous methylphenidate; rs-fMRI = resting-state functional MRI.